Ma et al. Nanoscale Research Letters (2018) 13:4
DOI 10.1186/s11671-017-2414-0

Nanoscale Research Letters

NANO EXPRESS Open Access

Atomic-Layer-Deposition of Indium Oxide Nano-films for Thin-Film Transistors

Qian Ma, He-Mei Zheng, Yan Shao, Bao Zhu, Wen-Jun Liu*, Shi-Jin Ding* and David Wei Zhang

Abstract

Atomic-layer-deposition (ALD) of In_2O_3 nano-films has been investigated using cyclopentadienyl indium (InCp) and hydrogen peroxide (H_2O_2) as precursors. The In_2O_3 films can be deposited preferentially at relatively low temperatures of 160–200 °C, exhibiting a stable growth rate of 1.4–1.5 Å/cycle. The surface roughness of the deposited film increases gradually with deposition temperature, which is attributed to the enhanced crystallization of the film at a higher deposition temperature. As the deposition temperature increases from 150 to 200 °C, the optical band gap (E_g) of the deposited film rises from 3.42 to 3.75 eV. In addition, with the increase of deposition temperature, the atomic ratio of In to O in the as-deposited film gradually shifts towards that in the stoichiometric In_2O_3, and the carbon content also reduces by degrees. For 200 °C deposition temperature, the deposited film exhibits an In:O ratio of 1:1.36 and no carbon incorporation. Further, high-performance In_2O_3 thin-film transistors with an Al_2O_3 gate dielectric were achieved by post-annealing in air at 300 °C for appropriate time, demonstrating a field-effect mobility of 7.8 $cm^2/V{\cdot}s$, a subthreshold swing of 0.32 V/dec, and an on/off current ratio of 10^7. This was ascribed to passivation of oxygen vacancies in the device channel.

Keywords: Atomic layer deposition, Low deposition temperature, In_2O_3, Thin-film transistors

Background

Indium oxide (In_2O_3) is a transparent metal oxide semiconductor, which exhibits a wide band gap of ~3.7 eV at room temperature, a high transparency for visible light, and excellent chemical stability [1, 2]. Therefore, In_2O_3 has been investigated for various applications such as photovoltaic devices, electrochemical sensors, and flat panel displays [3–5]. So far, several deposition techniques have been developed to prepare In_2O_3 thin-films, including sputtering [6, 7], sol-gel [8, 9], and chemical vapor deposition (CVD) [10, 11]. However, the techniques of sputtering and sol-gel usually suffer from a poor uniformity across a large area as well as inexact elemental composition; the CVD technique generally requires relatively high deposition temperatures of > 300 °C. These drawbacks make it challenging to achieve a uniform In_2O_3 film with precise thickness and composition control at a low deposition temperature.

In recent years, atomic-layer-deposition (ALD) has emerged as a promising approach that can yield excellent step coverage, atomic scale thickness controllability, good uniformity, and a relatively low deposition temperature. Accordingly, the growth of In_2O_3 thin-films has been explored by means of ALD with different precursors, including $InCl_3$-H_2O [12], $InCl_3$-H_2O_2 [13], InCp-O_3 [14], InCp-O_2-H_2O [15], and In $(CH_3)_3$-H_2O [16]. In terms of the precursors of $InCl_3$-H_2O and $InCl_3$-H_2O_2, the deposition temperatures for In_2O_3 films must be increased to ~ 300–500 °C [13]; meanwhile, the $InCl_3$ container should be heated to 285 °C in order to obtain ample $InCl_3$ vapor [15]. Furthermore, the byproduct of corrosive HCl can damage the ALD equipment and etch the deposited In_2O_3 film [17], and the growth rate of In_2O_3 is as low as 0.25–0.40 Å/cycle. Although other precursors such as TMIn-H_2O and TMIn-H_2O_2 have been adopted for ALD In_2O_3 films, the deposition temperatures are still high (i.e., 200–450 °C) in spite of relatively large growth rates (1.3–2 Å/cycle) [18].

In this work, InCp and H_2O_2 were proposed as the precursors of ALD In_2O_3 thin-films, thus the In_2O_3 thin-films were deposited successfully at lower temperatures,

* Correspondence: wjliu@fudan.edu.cn; sjding@fudan.edu.cn
State Key Laboratory of ASIC and System, Shanghai Institute of Intelligent Electronics and Systems, School of Microelectronics, Fudan University, Shanghai 200433, China

exhibiting a satisfactory growth rate. Additionally, the physical and chemical properties of the deposited films were characterized. Further, the In_2O_3 thin-film transistors (TFTs) with ALD Al_2O_3 gate dielectrics have been fabricated, demonstrating good electrical performance, such as a field effect mobility of 7.8 cm^2 V^{-1} s^{-1}, and an on/off current ratio of 10^7 etc.

Experimental

Si (100) wafers were cleaned using the standard Radio Corporation of America process, serving as the initial substrates. In_2O_3 thin-films were deposited onto the pre-cleaned Si (100) substrates using the ALD equipment (Wuxi MNT Micro Nanotech Co., LTD, China) at relatively low temperatures of 150–210 °C, where the temperatures of InCp (Fornano Electronic Technology Co., LTD, China, impurity: 99.999%) and H_2O_2 (30% aqueous solution) precursors were maintained at 130 and 50 °C, respectively. Nitrogen gas was used as a purging gas. To demonstrate the function of the ALD In_2O_3 thin-film, the In_2O_3-based channel TFTs were fabricated as the following processes. Firstly, a 38-nm Al_2O_3 gate dielectric film was grown on a pre-cleaned p-type Si (100) substrate (< 0.0015 Ω·cm) at 200 °C by ALD using trimethylaluminium and H_2O, and such low resistivity silicon substrate served as the back gate. Then, a 20-nm In_2O_3 channel layer was grown on the Al_2O_3 film at 160 °C. Source/drain contacts of Ti/Au (30 nm/70 nm) stacks were formed in turn by optical lithography, electron beam evaporation and a lift-off process. Finally, the fabricated devices were annealed at 300 °C in air for different times.

The crystallinity, surface morphology, elemental composition, absorption coefficient, and thickness of the In_2O_3 films were characterized by X-ray diffraction (XRD) (Bruker D8 Discover), atomic force microscopy (AFM) (Bruker Icon), X-ray photoelectron spectroscopy (XPS) (Kratos Axis Ultra DLD), ultraviolet-visible spectroscopy (UV-VIS), and ellipsometer (Sopra GES-SE, France), respectively. The electrical measurements of the devices were performed using a semiconductor parameter analyzer (B1500A, Agilent Technologies, Japan) with Cascade probe station in ambient air at room temperature.

Results and Discussion

Figure 1a shows the growth rate of the In_2O_3 film as a function of substrate temperature. It is found that a stable growth rate of ~ 1.46 Å/cycle is achieved in the range of 160 ~ 200 °C, revealing a fast growth rate and a well-defined temperature window for ALD In_2O_3 films. When the substrate temperature was reduced to 150 °C or increased to 210 °C, the resulting growth rate became larger [19, 20]. The former is attributed to the condensation of InCp on the substrate, whereas the latter is due to the thermal decomposition of InCp at a higher temperature. Further, the evolution of the deposited In_2O_3 film thickness was evaluated as a function of ALD cycles, as shown in Fig. 1b. It is clear that the In_2O_3 film thickness increases linearly with the number of deposition cycles, indicative of quite uniform growth.

To observe the evolution of the In_2O_3 film texture with deposition temperature, the XRD patterns of the In_2O_3 films deposited at different temperatures are presented in Fig. 2. When the deposition temperature does not exceed 160 °C, no diffraction peak can be observed. This indicates that the deposited In_2O_3 films at lower temperatures are amorphous. When the deposition temperature increases up to 170 °C, some diffraction peaks start to appear. Further, with the deposition temperature gradually increasing to 210 °C, the diffraction peak intensities increase dramatically, typically shown by the peaks at $2\theta = 30.3°$ and 35.4°. This indicates that the crystallinity and grain size of the as-deposited In_2O_3 film are enhanced gradually with increasing the deposition temperature. Figure 3 shows

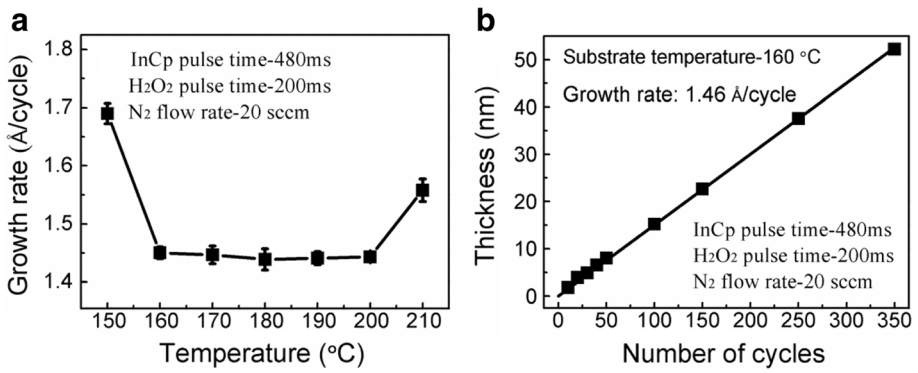

Fig. 1 **a** Growth rate of ALD In_2O_3 film on the Si substrate as a function of substrate temperature, and **b** dependence of the In_2O_3 film thickness on the number of ALD cycles at 160 °C

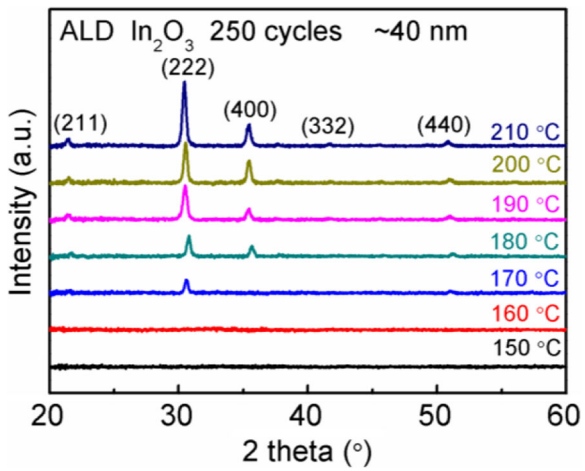

Fig. 2 X-ray diffraction patterns of the In_2O_3 films deposited at different temperatures for 250 cycles

the surface morphologies of the representative In_2O_3 films deposited at different temperatures. It is found that the film surface becomes rougher and rougher with increasing the deposition temperature, i.e., the resulting root-mean-square (RMS) roughness increases from 0.36 to 1.15 nm with increasing the deposition temperature from 160 to 210 °C. This should be related to the crystallinity of the In_2O_3 film. In terms of the deposition temperature of 160 °C, the deposited In_2O_3 film is amorphous, and it exhibits a very smooth surface. When the deposition temperature attains 180 °C, the deposited film becomes polycrystalline. This means that the resulting film contains lots of crystalline grains, and the grain sizes become larger and larger with increasing the deposition temperature, as revealed in Fig. 2. This is in good agreement with our observation that the sizes of hillocks on the film surface gradually increase with raising the deposition temperature, hence resulting in an increased RMS value.

Figure 4 shows high resolution C 1 s, In 3d and O1s XPS spectra of the In_2O_3 films deposited at different temperatures. Regarding the C 1 s XPS spectra shown in Fig. 4a, the film deposited at 160 °C displays a peak at 289.8 eV, which should correspond to C-O [21]. When the deposition temperature is increased to 180 °C, the peak becomes much weaker. Further, in terms of 200 °C deposition temperature, the C 1 s peak disappears. Thus, it is indicated that the higher the deposition temperature, the less the impurity of C in the deposited In_2O_3 film. Figure 4b depicts the In 3d XPS spectra of the In_2O_3 films, clearly demonstrating one-doublet Gaussian peaks at 444.7 and 452.3 eV, which are associated with In $3d_{5/2}$ and

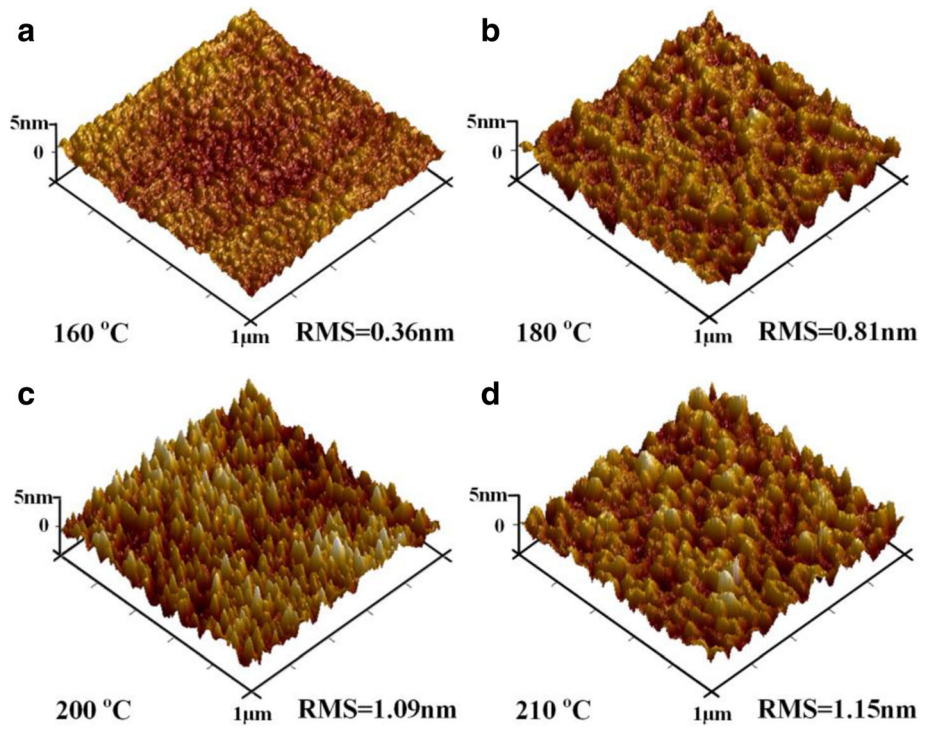

Fig. 3 The AFM images of the In_2O_3 films deposited at different temperatures: **a** 160 °C, **b** 180 °C, **c** 200 °C and **d** 210 °C. The deposition cycles were fixed at 250 for each film

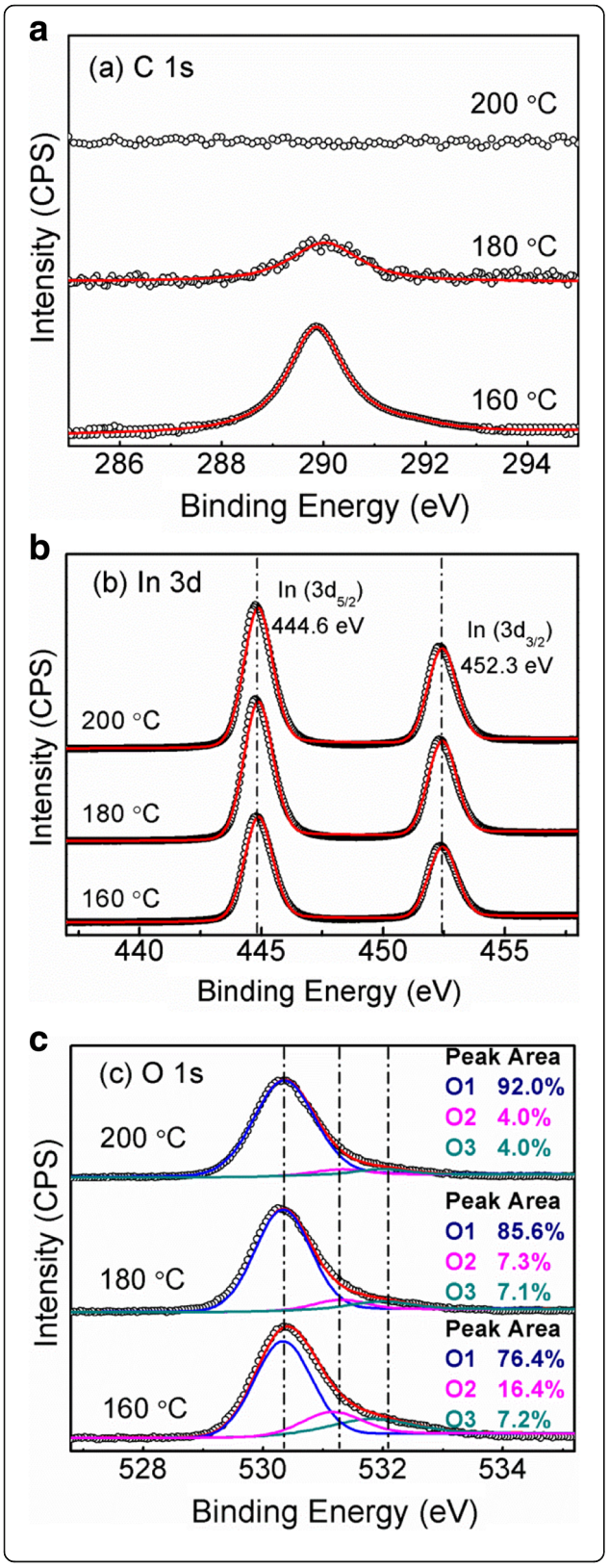

Fig. 4 High resolution **a** C 1s, **b** In 3d, and **c** O 1 s XPS spectra of the In_2O_3 films deposited at 160, 180, and 200 °C, respectively. To remove adventitious surface contaminants, all the samples were etched with in-situ Ar ion bombardment for 6 min before signal collection

In $3d_{5/2}$ core levels for In_2O_3 [22, 23]. The O 1 s XPS spectra are shown in Fig. 4c. It is found that the O 1 s spectrum for each sample can be well separated into three peaks, which are located at 529.8, 531.0, and 532.0 eV, respectively. These peaks correspond to O^{2-} ions bound with metal (O1), oxygen vacancies (O2) and –OH/CO (O3), respectively [24, 25]. As the deposition temperature increases from 160 to 200 °C, the relative percentage of O1 increases from 76 to 92%; and the relative percentage of O2 decreases gradually from 16 to 4%. Moreover, the relative percentage of O3 also exhibits a downward trend. These results indicate that a higher deposition temperature is beneficial to reduce the concentration of oxygen vacancies in the deposited film as well as hydroxyl groups and C–O bonds. Further, the elemental compositions of the In_2O_3 films deposited at different temperatures are listed in Table 1. Interestingly, the atomic ratio of In/O in the deposited film decreases by degrees with increasing deposition temperature. However, even for the pure In_2O_3 film deposited at 200 °C, the atomic ratio (1:1.36) of In/O is still larger than that (1:1.5) of the stoichiometric In_2O_3. This reveals that the ALD In_2O_3 film is generally rich in oxygen vacancies.

Figure 5a shows the variation of $(\alpha h\nu)^2$ as a function of photon energy for the as-deposited In_2O_3 films at different deposition temperatures. The optical band gap (E_g) of the In_2O_3 film can be determined by the Tauc's relation: $\alpha h\nu = A(h\nu - E_g)^n$ [26], where α is the absorption coefficient, A is a constant, h is the Plank constant, ν is the frequency, and the exponent n characterizes the nature of band transition. Here, $n = 1/2$, indicating that In_2O_3 is a semiconductor with a directly allowed transition. E_g is extracted by extrapolating the straight line portion to the energy bias at $\alpha = 0$. The extracted E_g for the In_2O_3 film is shown in Fig. 5b. It is seen that E_g increases from 3.42 to 3.75 eV with raising the deposition temperature from 150 to 200 °C. The increased E_g at higher deposition temperatures could result from the

Table 1 The Elemental Percentages of In_2O_3 Films Deposited at Different Temperatures

Deposition Temperature	C	In	O	Atomic Ratio of In:O
160 °C	6.9%	42.9%	50.2%	1:1.17
180 °C	1.1%	42.3%	56.5%	1:1.34
200 °C	0	42.3%	57.7%	1:1.36

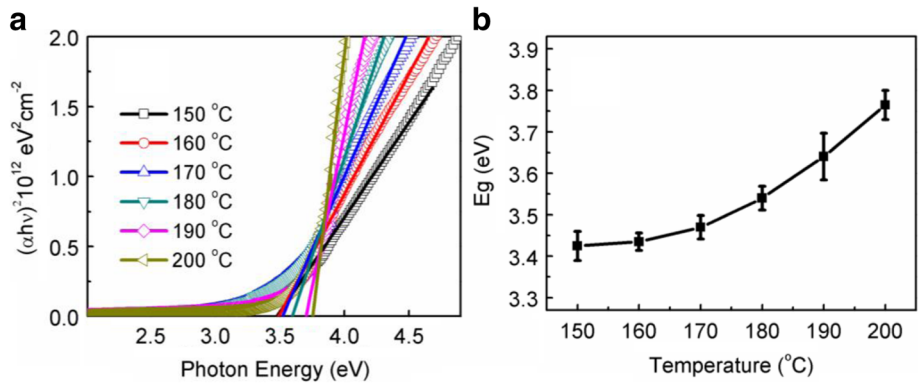

Fig. 5 a Plotting of $(\alpha h\nu)^2$ vs photon energy for the In_2O_3 films deposited at different temperatures; **b** dependence of the extracted band gap (E_g) of In_2O_3 on deposition temperature

reductions of oxygen vacancies and C impurity in the deposited film. In fact, other researchers also reported that when lots of oxygen vacancies existed in ZnO, the impurities states became more delocalized and overlapped with the valence band edge, thus leading to the band gap narrowing [27]. In addition, the gradually enhanced crystallinity as a function of deposition temperature could influence the optical band gap of the In_2O_3 film. This can be explained as follows. As the deposition temperature rises, the grain size of the deposited In_2O_3 film increases, shown in Fig. 2. This thus leads to a decrease in the density of grain boundaries in the film. Since electrons are easily trapped in the grain boundaries, the number of free electrons should increase in the In_2O_3 film with less grain boundaries [28, 29]. Therefore, such an increased electron concentration results in a larger optical band gap due to the Burstein-Moss shift [30].

To demonstrate the function of the ALD In_2O_3 film acting as the channel of TFT, the In_2O_3-channel-based TFTs with atomic-layer-deposited Al_2O_3 gate dielectrics were fabricated. Figure 6a shows the transfer characteristics of In_2O_3 TFTs. It is found that the as-fabricated device does not exhibit the switch characteristics typical of field-effect transistors, but a conductor-like between source and drain. This should be attributed to the existence of lots of oxygen vacancies in the In_2O_3 channel because oxygen vacancies can supply free electrons. Therefore, for the sake of reducing the concentration of oxygen vacancies in the In_2O_3 channel, post-annealing in air was carried out at 300 °C. It is clear that the In_2O_3 TFT exhibits a typical switching behavior after 2-h annealing. This indicates that the post-annealing in air can improve significantly the device performance. Further, as the annealing time increases gradually to 10 h, the threshold voltage (V_{th}) of the TFT shifts in the direction of positive bias, and the sub-threshold swing (SS) improves little by little. However, when the annealing time increases to 11 h, the device performance starts to degenerate. It is noted that hydrogen may be incorporated into the film during the fabrication process, acting as an electron trap by forming –OH bonds in the channel or

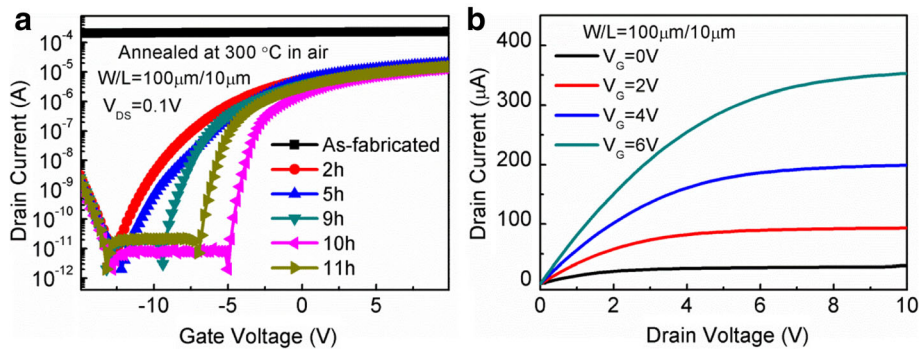

Fig. 6 a Transfer characteristics of the In_2O_3 TFTs annealed at 300 °C in air for different time; **b** Output characteristics of the In_2O_3 TFT annealed at 300 °C in air for 10 h

at the interface between the channel and dielectric [31]. These electron traps perhaps result in the degradation of SS. After annealing in air, the OH bonds were reduced by incorporation of O_2 molecules [32]. This could lead to a decrease in the trap density, thus improving the SS of the device. In terms of 10 h annealing in air, the In_2O_3 TFT exhibits a field-effect mobility (μ_{EF}) of 7.8 $cm^2 V^{-1} s^{-1}$, a V_{th} of −3.7 V, a SS of 0.32 V/dec, and an on/off current ratio (I_{on}/I_{off}) of 10^7. The corresponding output characteristics are also presented in Fig. 6b, demonstrating clear pinch-off and current saturation behaviors under various positive gate voltages. Furthermore, the output curves also indicate an *n*-type enhancement mode. For comparison, Table 2 summarizes the characteristics of the reported ALD In_2O_3 films and TFTs from different research groups [33–37]. It is demonstrated that our In_2O_3 film shows a superior growth rate at a relatively low temperature, and the fabricated device also exhibits a small SS. However, the general performance of the device is not so perfect, which could be improved via some process and device structure optimizations.

To well understand the influence of post-annealing in air on the composition of the In_2O_3 channel, the In_2O_3 films were annealed at 300 °C for different times, and then were analyzed by means of XPS. Table 3 lists the elemental percentages of various annealed films. As the annealing time increases from 2 to 11 h, the atomic ratio of In:O decreases from 1:1.22 to 1:1.48, gradually approaching that (1:1.5) of the stoichiometric In_2O_3. This further confirms that increasing annealing time in air effectively reduced the density of oxygen vacancies in the In_2O_3 film. Therefore, the improvement in the performance of the In_2O_3 TFT should be mainly attributed to the passivation of oxygen vacancies which could be located in the bulk channel and/or the interface between the channel and the dielectric [25]. However, the excessive annealing degraded the performance of the device, as revealed by 11 h annealing. This could be ascribed to the change of crystallization of the In_2O_3 channel layer as well as possible oxidation of Ti electrodes during superfluous post-annealing in air. Thus, an appropriate annealing time is required in order to achieve good performance of the In_2O_3 TFT.

Table 3 The Elemental Percentages of In_2O_3 Films Annealed at 300 °C in Air for Different Time

Annealing time	C	In	O	In:O
2 h	5.9%	42.4%	51.7%	1:1.22
7 h	6.2%	41.6%	52.2%	1:1.25
10 h	6.3%	39.8%	53.9%	1:1.35
11 h	4.8%	38.4%	56.8%	1:1.48

All the films were deposited at 160 °C and etched with in-situ Ar ion bombardment

Conclusions

The fast ALD growth of the In_2O_3 films has been achieved at relatively low temperatures (160–200 °C) with the InCp and H_2O_2 precursors, exhibiting a uniform growth rate of 1.46 Å/cycle. As the deposition temperature increased, the crystallization of the deposited film was enhanced gradually. Meanwhile, both oxygen vacancies and carbon impurities in the deposited films were also reduced significantly. This thus led to an increase in the E_g of In_2O_3. Further, with the ALD In_2O_3 channel layer, the TFTs with an ALD Al_2O_3 dielectric were fabricated. As the post-annealing time in air was lengthened, the electrical performance of the In_2O_3 TFT was improved distinctly till 10 h annealing. This is mainly due to the passivation of oxygen vacancies located in the bulk channel and/or the interface between the channel and the dielectric after annealing in air. In terms of 10 h annealing, the device exhibited good

Table 2 Characteristics of the ALD In_2O_3 Films and In_2O_3 TFTs From Different Groups

Oxygen Precursor	Metal Precursor	Deposition Temperature (°C)	Growth rate (Å/cycle)	Channel Thickness (nm)	μ ($cm^2/V{\cdot}s$)	V_{TH} (V)	I_{ON}/I_{OFF}	SS (V/dec)	Ref.
H_2O	$Et_2InN(TMS)_2$[a]	175~250	0.7	–	–	–	–	–	[23]
H_2O	DMLDMIn[b]	300~350	0.6	–	–	–	–	–	[33]
O_2 plasma	$Et_2InN(SiMe_3)_2$[c]	250	1.45	5	39.2	−1.18	–	0.27	[34]
H_2O	TMIn[d]	200~251	0.39	–	–	–	–	–	[35]
H_2O_2	InCA-1[e]	125	0.6	18	15	−0.2	10^8	–	[36]
H_2O_2	InCA-1[e]	150	0.6	18	9.8	−0.2	10^9	0.63	[37]
H_2O_2	InCp	160	1.46	20	7.8	−3.7	10^7	0.32	This work

[a]$Et_2InN(TMS)_2$ represents the diethyl [bis (trimethylsilyl) amido]- indium
[b]DMLDMIn represents the dimethylamino-dimethylindium
[c]$Et_2InN(SiMe_3)_2$ represents the diethyl [bis (trimethylsilyl) amido] indium
[d]TMIn represents the trimethyl indium
[e]InCA-1 represents the [1,1,1-trimethyl-N-(trimethylsilyl) silanaminato]-Indium

performance such as a field-effect mobility of 7.8 $cm^2/V{\cdot}s$, a subthreshold swing of 0.32 V/dec, and an on/off current ratio of 10^7. In terms of 200 °C deposition temperature, the deposited film exhibits an In:O ratio of 1:1.36 without detectable carbon, thus revealing the existence of oxygen vacancies in the as-deposited film.

Acknowledgements
This work was supported by the National Key Technologies R&D Program of China (2015ZX02102-003) and the National Natural Science Foundation of China (61274088, 61774041). This work was also sponsored by Shanghai Pujiang Program (16PJ1400800), China.

Authors' Contributions
QM carried out the ALD growth of In_2O_3 nano-films, and the characterization of films and TFTs. SJD and WJL supervised the work and drafted the manuscript. HMZ, YS, BZ, and DWZ helped to analyze the experimental results. All authors read and approved the final manuscript.

Competing Interests
The authors declare that they have no competing interests.

Publisher's Note

Received: 21 September 2017 Accepted: 17 December 2017
Published online: 09 January 2018

References

1. Kraini M, Bouguila N, Halidou I, Timoumi A, Alaya S (2013) Properties of In_2O_3 films obtained by thermal oxidation of sprayed In_2S_3. Mat Sci Semicon Proc 16:1388–1396
2. Savarimuthu E, Lalithambika KC, Raj AME, Nehru LC, Ramamurthy S (2007) Synthesis and materials properties of transparent conducting In_2O_3 films prepared by sol-gel-spin coating technique. J Phys Chem Solids 68:1380–1389
3. Gorrn P, Sander M, Meyer J, Kroger M, Becker E, Johannes HH et al (2006) Towards see-through displays: fully transparent thin-film transistors driving transparent organic light-emitting diodes. Adv Mater 18:738–741
4. Park JS, Kim K, Park YG, Mo YG, Kim HD, Jeong JK (2009) Novel ZrInZnO thin-film transistor with excellent stability. Adv Mater 21:329–333
5. DY K, Kim IH, Lee I, Lee KS, Lee TS, Jeong JH et al (2006) Structural and electrical properties of sputtered indium-zinc oxide thin films. Thin Solid Films 515:1364–1369
6. Cho S (2012) Effects of rapid thermal annealing on the properties of In_2O_3 thin films grown on glass substrate by rf reactive magnetron sputtering. Microelectron Eng 89:84–88
7. Hotovy I, Pezoldt J, Kadlecikova M, Kups T, Spiess L, Breza J et al (2010) Structural characterization of sputtered indium oxide films deposited at room temperature. Thin Solid Films 518:4508–4511
8. Tahar RBH, Ban T, Ohya Y, Takahashi Y (1997) Optical, structural, and electrical properties of indium oxide thin films prepared by the sol-gel method. J Appl Phys 82:865–870
9. King PDC, Veal TD, Fuchs F, Wang CY, Payne DJ (2009) Band gap, electronic structure, and surface electron accumulation of cubic and rhombohedral In_2O_3. Phys Rev B 79:205211
10. Nishino J, Kawarada T, Ohshio S, Saitoh H, Maruyama K (1997) Conductive indium-doped zinc oxide films prepared by atmospheric-pressure chemical vapour deposition. J Mater Sci 16:629–631
11. Girtan M, Folcher G (2003) Structural and optical properties of indium oxide thin films prepared by an ultrasonic spray CVD process. Surf Coat Tech 172: 242–250
12. Elam JW, Libera JA, Hryn JN (2011) Indium oxide ALD using Cyclopentadienyl indium and mixtures of H_2O and O_2. J Electro Chem Soc 41:147–155
13. Asikainen T, Ritala M, Leskela M (1994) Growth of In_2O_3 thin films by atomic layer epitaxy. J Electrochem Soc 141:3210–3213
14. Nilsen O, Balasundaraprabhu R, Monakhov EV, Muthukumarasamy N, Fjellvag H, Svensson BG (2009) Thin films of In_2O_3 by atomic layer deposition using $in(acac)_3$. Thin Solid Films 517:6320–6322
15. Elam JW, Martinson ABF, Pellin MJ, Hupp JT (2006) Atomic layer deposition of In_2O_3 using cyclopentadienyl indium: a new synthetic route to transparent conducting oxide films. Chem Mater 18:3571–3578
16. Ott AW, Johnson JM, Klaus JW, George SM (1997) Surface chemistry of In_2O_3 deposition using $in(CH_3)_3$ and H_2O in a binary reaction sequence. Appl Surf Sci 112:205–215
17. Kim H (2003) Atomic layer deposition of metal and nitride thin films: current research efforts and applications for semiconductor device processing. J Vac Sci Technol B 21:2231–2261
18. Brahim C, Chauveau F, Ringuede A, Cassir M, Putkonen M (2009) ZrO_2-In_2O_3 thin layers with gradual ionic to electronic composition synthesized by atomic layer deposition for SOFC applications. J Mater Chem 19:760–766
19. Maeng WJ, Choi DW, Park J, Park JS (2015) Atomic layer deposition of highly conductive indium oxide using a liquid precursor and water oxidant. Ceram Int 41:10782–10787
20. Maeng WJ, Choi DW, Park J, Park JS (2015) Indium oxide thin film prepared by low temperature atomic layer deposition using liquid precursors and ozone oxidant. J Alloy Compd 649:216–221
21. Mane AU, Allen AJ, Kanjolia RK, Elam JW (2016) Indium oxide thin films by atomic layer deposition using trimethylindium and ozone. J Phys Chem 120:9874–9883
22. Acacia N, Barreca F, Barletta E, Spadaro D, Curro G, Neri F (2010) Laser ablation synthesis of indium oxide nanoparticles in water. Appl Surf Sci 256: 6918–6922
23. Maeng WJ, Choi DW, Chung KB, Koh W, Kim GY, Choi SY, Park JS (2014) Highly conducting, transparent, and flexible indium oxide thin film prepared by atomic layer deposition using a new liquid precursor $Et_2InN(SiMe_3)_2$. Appl Mater Interfaces 4:17481–17488
24. Zheng LL, Ma Q, Wang YH, Liu WJ, Ding SJ, Zhang W (2016) High-performance unannealed a-InGaZnO TFT with an atomic-layer-deposited SiO_2 insulator. IEEE Electron Device Lett 37:743–746
25. Wang YH, Ma Q, Zheng LL, Liu WJ, Ding SJ, Lu HL et al (2016) Performance improvement of atomic layer-deposited ZnO/Al_2O_3 thin-film transistors by low-temperature annealing in air. IEEE Trans Electron Dev 63:1893–1898
26. Lu HL, Scarel G, Alia M, Fanciulli M, Ding SJ (2008) Spectroscopic ellipsometry study of thin NiO films grown on Si (100) by atomic layer deposition. Appl Phys Lett 92:222907
27. Wang JP, Wang ZY, Huang BB, Ma YD, Liu YY, Qin XY et al (2012) Oxygen vacancy induced band-gap narrowing and enhanced visible light photocatalytic activity of ZnO. Appl Mater Interfaces 4:4024–4030
28. Fallah HR, Ghasemi M, Hassanzadeh A (2007) Influence of heat treatment on structural, electrical, impedance and optical properties of nanocrystalline ITO films grown on glass at room temperature prepared by electron beam evapovation. Phys E 39:69–74
29. Han H, Mayer JW, Alford TL (2006) Band gap shift in the indium-tin-oxide films on polyethylene napthalate after thermal annealing in air. J Appl Phys 100:083715
30. Sarhaddi R, Shahtahmasebi N, Rezaee M, Bagheri MM (2010) Effect of post-annealing temperature on nano-structure and energy band gap of indium tin oxide (ITO) nano-particles synthesized by polymerizing-complexing sol-gel method. Phys E 43:452–457
31. Huby N, Ferrari S, Guziewicz E, Godlewski M, Osinniy V (2008) Electrical behavior of zinc oxide layers grown by low temperature atomic layer deposition. Appl Phys Lett 92:023502
32. Lee S, Bang S, Park J, Park S, Jeong W, Jeon H (2010) The effect of oxygen remote plasma treatment on ZnO TFTs fabricated by atomic layer deposition. Phys Status Solidi A 207:1845–1849
33. Kim D, Nam T, Park J, Gatineau J, Kim H (2015) Growth characteristics and properties of indium oxide and indium-doped zinc oxide by atomic layer deposition. Thin Solid Films 587:83–87
34. Yeom HI, Ko JB, Mun G, Park SK (2016) High mobility polycrystalline indium oxide thin-film transistors by means of plasma-enhanced atomic layer deposition. J Mater Chem C 4:6873–6880
35. Lee DJ, Kwon JY, Lee JI, Kim KB (2011) Self-limiting film growth of transparent conducting In_2O_3 by atomic layer deposition using trimethylindium and water vapor. J Phys Chem C 115:15384–15389

36. Sheng JZ, Choi DW, Lee SH, Park J, Park JS (2016) The modulated performances of transparent ALD indium oxide thin films on flexible substrate: a transition between metal-like conductor and high performance semiconductor. J Mater Chem C 4:7571–7576
37. Sheng JZ, Park J, Choi DW, Lim J, Park JS (2016) A study on the electrical properties of atomic layer deposition grown InO_X on flexible substrates with respect to N_2O plasma treatment and the associated thin-film transistor behavior under repetitive mechanical stress. Appl Mater Interfaces 8:31136–31143